4. Nanoconfined water for environmental applications

4.1. Introduction to Carbon Nanotube Arrays

Carbon Nanotubes (CNTs) and other carbon-based particles are used as fillers in a large variety of composite materials, because of their superior thermal, mechanical and electrical properties [43, 67, 134, 178, 360].

Patterns of vertically-aligned CNTs (also known as Carbon Nanotube Arrays – CNAs) can be immersed in polymer or ceramic matrices for obtaining nanoporous materials, which are characterized by precisely controlled pore width and density. CNAs are typically produced by either physical [361] or chemical [362, 363] vapor deposition on catalyst or substrate patterns predesigned by nanolithography processes; however, alternative production approaches - such as self-assembly on biological templates [364] or DNA-mediated [365] - have also been recently proposed. Well-ordered nanoporous membranes are obtained by CNAs incorporation across polymer or ceramic matrices by spin-coating [366] or conformal encapsulation [367], respectively. Plasma-etching treatments can then open up CNT tips, whereas plasma-oxidation processes functionalize channel entrances for gatekeeping purpose [368].

CNA-based materials may find biomedical or engineering applications such as nanostructured filters, separators, detectors or vectors with diagnostic or therapeutic function. Concerning biomedical applications, CNAs are ideal building blocks for designing artificial biomembranes capable of mimicking functionalities of Nature's channels (e.g. aquaporins), as recently investigated both experimentally [369] and numerically [370]. These nanoporous materials are also used in devices for controlled transdermal drug delivery [371] as well as for DNA/RNA amplification [364], sensing [372] or translocation [373–375]. Engineering applications of CNAs mainly exploit their ability to selectively trap nanoimpurities (e.g. wastewater treatments [376, 377]) or ions (e.g. seawater desalination [13, 90, 378, 379])

dispersed in water, as well as their gas separation [380] and catalysis properties [381], especially for fuel cell technology. Further peculiar properties of CNTs entail an even broader applicability of CNAs in engineering: super-hydrophobicity for self-cleaning surfaces [382, 383]; phonon dragging by fluid flow for energy harvesting or nanosensing [384, 385]; optical properties for electrical coupling in photonic [386] or photothermal devices [364].

Although mechanical, thermal and electrical properties of CNTs have been deeply investigated [134, 135], a complete physical understanding of the diffusion properties of fluids through their pores is still incomplete [15, 139]. Transport diffusivity D_T of water inside narrow CNTs is order of magnitude faster than bulk one, as demonstrated by both computational calculations and experiments [368, 369, 387–389]. Such flow rate enhancement is due to slip flow conditions of water within CNT nanopores, which is governed by the liquid structure and collective molecular motion induced by both mechanical and electrical smoothness of CNT walls and their confinement effect on water. However, the enhanced D_T of water in narrow cavities is usually not accompanied by an analogous D increase, especially in case of single-file diffusion [15]. Hence, predicting the water self-diffusivity (i.e. mobility) D under nanoconfined conditions is also of interest in several fields [27, 43], whereas novel and improved experimental techniques may further support these studies in the near future [15].

Based on the scaling law for the water mobility under nanoconfined conditions presented in Chapter 2, novel strategies for precise modulation of water diffusion within membranes made of Carbon Nanotube Arrays are envisioned in this Chapter. First, a theoretical introduction to mass diffusion at the nanoscale is presented, then results of Molecular Dynamics (MD) of water self-diffusivity in Carbon Nanotube Arrays are shown. In a first approach, the water self-diffusion coefficient may be tuned by finely controlling the size distribution of the pore size. In the second approach, D can be varied at will by means of externally induced electrostatic fields. Results pave the way to a precise design of transport properties of water in CNA-based devices.

Starting from the latter strategy, switchable molecular sieves are proposed, where membranes are properly designed with sieving and permeation features that can be dynamically activated/deactivated. Areas where a precise control of water transport properties is beneficial range from energy and environmental engineering up to nanomedicine.

4.2. Diffusion at the nanoscale

In this Section, self-diffusion coefficient D_i, transport (Fick's) diffusion coefficient $D_{T,i}$, Maxwell-Stefan (M-S) diffusion coefficients $Đ_i$ and $Đ_{ii}$ of the $i-th$ species are defined in case of mass transport at the nanoscale, and their mutual relations derived. Finally, the latter relations are used for correlating self- and transport diffusivity of water in CNTs.

4.2.1. Diffusivities at molecular level

In molecular mechanics methods, the mass transfer of the *i-th* mixture component is quantified by self-diffusion coefficient

$$D_i = \frac{1}{2} \lim_{\Delta t \to \infty} \frac{1}{n_i \Delta t} \sum_{l=1}^{n_i} \left\| \mathbf{r}_{l,i}\left(t + \Delta t\right) - \mathbf{r}_{l,i}\left(t\right) \right\|^2, \tag{4.1}$$

which is obtained by computing the mean square displacement of individual molecules and it reflects a combination of molecule-molecule and molecule-wall collisions, and by Maxwell-Stefan (M-S) diffusion coefficient

$$Đ_i = \frac{1}{2} \lim_{\Delta t \to \infty} \frac{1}{n_i \Delta t} \left\| \sum_{l=1}^{n_i} \mathbf{r}_{l,i}\left(t + \Delta t\right) - \mathbf{r}_{l,i}\left(t\right) \right\|^2, \tag{4.2}$$

which is obtained by computing the mean square displacement of an ensemble of molecules and it characterizes only molecule-wall interactions [390–393]. Moreover, M-S equations allow also to define the self-exchange coefficient $Đ_{ii}$, which is a molecular diffusivity only influenced by molecule-molecule interactions, as it will be deepened later on.

For matching molecular mechanics and experimental results, it is useful to define the transport (Fick's) diffusion coefficient of the *i-th* mixture component as

$$D_{T,i} = -\frac{\mathbf{J}_i}{\nabla c_i} \longrightarrow \mathbf{J}_i = -D_{T,i} \nabla c_i, \tag{4.3}$$

which is related to D_i, $Đ_i$ and $Đ_{ii}$ by

$$D_{T,i} = \Gamma_i \left(\frac{1}{D_i} - \frac{1}{Đ_{ii}} \right)^{-1}, \tag{4.4}$$

where Γ_i is the thermodynamic factor, which can be understood as an extra driving force for transport diffusion as it will be demonstrated in the followings (see Equation 4.22).

4.2.2. Maxwell-Stefan equations

Let us assume an ideal gas binary mixture; under the hypothesis of elastic collisions and no shear stress (negligible velocity gradient), the momentum conservation in a given ensemble of particles is:

The sum of the forces acting on molecules of type 1 per unit volume	$\propto$	The rate of change of momentum of the molecules of type 1 per unit volume	$=$	average amount of momentum exchanged in a single collision	$\times$	number of $1-2$ collisions per unit volume per unit time
				$(\mathbf{u}_1 - \mathbf{u}_2)$		$x_1 x_2$

If constant pressure P is considered in a system's box with S surface, the force acting on the species 1 in z plane is $Sp_1|_z$ ($p_1 = x_1 P$ is the partial pressure of species 1), whereas the force acting on the species 1 in the $z + \Delta z$ plane is $-Sp_1|_{z+\Delta z}$ [394]. Therefore, the net force acting on the species 1 molecules is $S\left(p_1|_z - p_1|_{z+\Delta z}\right)$. Dividing by the volume $S\Delta z$, taking the limit as $\Delta z \to 0$ and adding the contributions from the other two spacial dimensions, the net force $\mathbf{F}_{V,1}$ acting on species 1 molecules per unit volume is

$$\mathbf{F}_{V,1} = -\nabla p_1. \tag{4.5}$$

Hence, the momentum conservation for species 1 molecules can be now reformulated as

$$-\nabla p_1 \propto (x_1, x_2, (\mathbf{u}_1 - \mathbf{u}_2)) \tag{4.6}$$

where the mole fraction of the $i-th$ species is $x_i = \frac{c_i}{c_t}$ and $\sum_{i=1}^{n} x_i = 1$. By introducing a proportionality factor f_{12}, Equation 4.6 becomes

$$\nabla p_1 = -f_{12} x_1 x_2 \left(\mathbf{u}_1 - \mathbf{u}_2\right); \tag{4.7}$$

therefore ∇p_1 is the actual force exerted per unit volume of the mixture trying to move species 1 through the molecules of species 2 at a relative velocity $(\mathbf{u}_1 - \mathbf{u}_2)$, $x_1 x_2$ is a concentration weight factor and f_{12} is analogous to a friction factor or drag coefficient [394]. A pictorial representation of the interaction between the molecules of species 1 and 2 is provided in Figure 4.1.

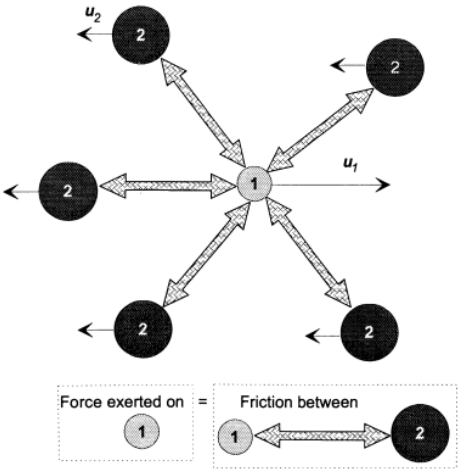

Figure 4.1.: Force balance in M-S diffusion phenomena in a binary system. Picture taken from Reference [394]

Finally, by defining Maxwell-Stefan diffusivity as $Đ_{12} = P/f_{12}$, Equation 4.7 can be rewritten as

$$\mathbf{d}_1 \equiv \left(\frac{1}{P}\right) \nabla p_1 = -\frac{x_1 x_2 \left(\mathbf{u}_1 - \mathbf{u}_2\right)}{Đ_{12}}, \tag{4.8}$$

where $\mathbf{d}_i$ is the driving force for diffusion of the $i-th$ species in an ideal gas mixture at constant temperature and pressure. Equation 4.8 is the Maxwell-Stefan (M-S) equation for the diffusion of species 1 in a binary ideal gas mixture, and it can be analogously defined for species 2. Note that, if pressure is constant across the diffusion path, $\mathbf{d}_i = (1/P)\nabla p_i = \nabla x_i$. Moreover, since $\nabla x_1 + \nabla x_2 = 0$, it derives that M-S binary diffusion coefficients are symmetric: $Đ_{12} = Đ_{21}$.

For mixtures containing n species, Equation 4.8 can be generalized as

$$\mathbf{d}_i = -\sum_{j=1}^{n} \frac{x_i x_j \left(\mathbf{u}_i - \mathbf{u}_j\right)}{Đ_{ij}}. \tag{4.9}$$

By defining the molar flux as $\mathbf{N}_i = c_i \mathbf{u}_i$, Equation 4.9 becomes

$$\mathbf{d}_i = \sum_{j=1}^{n} \frac{(x_i \mathbf{N}_j - x_j \mathbf{N}_i)}{c_t \mathcal{D}_{ij}}, \tag{4.10}$$

or, in terms of the molar diffusion flux $\mathbf{J}_i = c_i (\mathbf{u}_i - \mathbf{u})$, where $\mathbf{u} = \sum_{i=1}^{n} x_i \mathbf{u}_i$ is the molar average velocity:

$$\mathbf{d}_i = \sum_{j=1}^{n-1} \nabla x_j = \sum_{j=1}^{n} \frac{(x_i \mathbf{J}_j - x_j \mathbf{J}_i)}{c_t \mathcal{D}_{ij}}, \tag{4.11}$$

namely the M-S diffusion equations for multicomponent systems.

The much higher density of liquids and dense gases means that we can no longer safely assume that only binary (two molecule) collisions take place; three (or more) molecule collisions occur sufficiently frequently in liquids and dense gases and contribute to the momentum transfer process. However, Equation 4.11 applies equally to gases and liquids: if the constituents (i and j) are in relative motion each other and, therefore, moving at different velocities ($\mathbf{u}_i$ and $\mathbf{u}_j$), we may expect composition gradients to be setup in the system as a result of the frictional drag of one set of molecules moving through the other. It does not matter whether this frictional drag arises purely from intermolecular collisions, as in the kinetic theory of gases, or from intermolecular forces acting between the two sets of molecules. Therefore, Equation 4.11 holds also in nonideal fluids, and $\mathcal{D}_{ij}$ has the same physical significance as an inverse drag coefficient [394].

However, for nonideal fluids $\mathbf{d}_i$ is defined as

$$\mathbf{d}_i \equiv \frac{x_i}{RT} \nabla_{T,P} \mu_{c,i}, \tag{4.12}$$

where temperature and pressure are fixed and $\mu_{c,i} = \mu^0_{c,i}(T) + RT \ln(a_i)$ is the molar chemical potential, $a_i = x_i \gamma_i$ the fluid activity and γ_i the activity coefficient. Note that, in case of dense gases, $a_i = \phi_{a,i}$, where $\phi_{a,i} = f_i / p_i$ is the fugacity coefficient of the $i - th$ component [394].

According to Reference [25], $d_{i,x}$ can be then rewritten as:

$$\begin{aligned} d_{i,x} &= \frac{x_i}{RT}\frac{\partial \mu_{c,i}}{\partial x} \\ &= \frac{x_i}{RT}\left(\frac{\partial \mu^0_{c,i}(T)}{\partial x} + \frac{\partial RT\ln\left(x_i\gamma_i\right)}{\partial x}\right) \\ &= \frac{x_i}{RT}\left(RT\frac{1}{x_i\gamma_i}\frac{\partial\left(x_i\gamma_i\right)}{\partial x}\right) \\ &= \frac{1}{\gamma_i}\left(x_i\frac{\partial\gamma_i}{\partial x} + \gamma_i\frac{\partial x_i}{\partial x}\right) \\ &= \frac{\partial x_i}{\partial x}\left(1 + \frac{x_i}{\gamma_i}\frac{\partial\gamma_i}{\partial x_i}\right) \\ &= \frac{\partial x_i}{\partial x}\left(1 + \frac{\partial\ln\gamma_i}{\partial\ln x_i}\right) \end{aligned} \tag{4.13}$$

Therefore, if the thermodynamic factor is defined as

$$\Gamma_i \equiv 1 + \frac{\partial\ln\gamma_i}{\partial\ln x_i}, \tag{4.14}$$

or, in case of dense gases

$$\Gamma_i \equiv 1 + \frac{\partial\ln\phi_{a,i}}{\partial\ln x_i}, \tag{4.15}$$

by combining Equations 4.11, 4.12, 4.13 and 4.14, M-S equation for non-ideal fluids takes the final form:

$$\mathbf{d}_i = \sum_{j=1}^{n-1}\Gamma_{ij}\nabla x_j = \sum_{j=1}^{n}\frac{\left(x_i\mathbf{J}_j - x_j\mathbf{J}_i\right)}{c_t Đ_{ij}}. \tag{4.16}$$

For practical reasons, the thermodynamic factor may be also conventionally taken as [390]:

$$\Gamma_i \equiv \frac{\partial\ln f_i}{\partial\ln c_i} = \frac{c_i}{f_i}\frac{\partial f_i}{\partial c_i}. \tag{4.17}$$

When the mixture is made up of almost identical species, $Đ_{ij} = Đ_i$. Therefore, if Equation 4.3 and 4.16 are compared, it can be easily deduced that Fick and M-S diffusivities are interrelated as

$$D_{T,i} = \Gamma_i Đ_i. \tag{4.18}$$

By factoring out the thermodynamic influence, the $Đ_i$ can be obtained from experimental data on the Fick's $D_{T,i}$, and it is for this reason that $Đ_i$ is also referred to as the *corrected diffusivity*. From a molecular standpoint, $Đ_i$ is a reflection of facility for collective motion of molecules and can be determined, for example, from MD simulations of displacements in each of the coordinate directions (see Equation 4.2).

For this reason, the Maxwell-Stefan's $Đ_i$ is amenable to simpler interpretation than the $D_{T,i}$, because it can be related to the fundamental process of molecular jumps [390].

4.2.3. Correlations between diffusivities in nanoporous materials

Equation 4.16 can be reshaped as

$$-\frac{c_i}{RT}\nabla\mu_{c,i} = \sum_{\substack{j=1 \\ j\neq i}}^{n} \frac{x_j\mathbf{N}_i - x_i\mathbf{N}_j}{Đ_{ij}} + \frac{\mathbf{N}_i}{Đ_i}, \qquad i = 1,2,...,n \tag{4.19}$$

which unveils an easier interpretation of diffusion phenomena: $Đ_i$ has the same physical meaning as for unary diffusion, and it characterizes species $i-wall$ interactions in the broadest sense; $Đ_{ij}$ are exchange coefficients representing interactions between components i with component j. At the molecular level, the $Đ_{ij}$ reflect how the facility for transport of species i correlates with that of species j. As already demonstrated, $Đ_{ij} = Đ_{ji}$.

Starting from the previous considerations, self-diffusion coefficient of the $i-th$ species can be now analyzed with a better physical understanding. In fact, let us consider equimolar diffusion ($\mathbf{N}_1 + \mathbf{N}_2 = 0$) in a system consisting of two species, tagged and untagged, that are identical with respect to diffusional properties. Hence, Equation 4.19 becomes:

$$-\frac{c_1}{RT}\nabla\mu_{c,1} = \frac{(x_1+x_2)\,\mathbf{N}_1}{Đ_{11}} + \frac{\mathbf{N}_1}{Đ_1} = \left(\frac{1}{Đ_{11}} + \frac{1}{Đ_1}\right)\mathbf{N}_1, \tag{4.20}$$

while self-diffusion coefficient D_i within a pore is defined as

$$-\frac{c_i}{RT}\nabla\mu_{c,i} = \frac{\mathbf{N}_i}{D_i}. \tag{4.21}$$

Hence, in general we obtain

$$\frac{1}{D_i} = \frac{1}{Đ_i} + \frac{1}{Đ_{ii}}, \tag{4.22}$$

or, in a n-component mixture,

$$\frac{1}{D_i} = \frac{1}{Đ_i} + \frac{x_i}{Đ_{ii}} + \sum_{\substack{j=1 \\ j \neq i}}^{n} \frac{x_j}{Đ_{ij}}. \qquad i = 1, 2, ..., n \tag{4.23}$$

In other words, self-diffusivity D_i within a pore (or, analogously, self-diffusion drag resistance $1/D_i$) is dictated by (a) species i-wall, (b) species i - species i, and (c) species i - species j interactions [390]. If Equations 4.22 and 4.18 are considered, Equation 4.4 can be finally obtained from [395]

$$\begin{cases} \frac{1}{D_i} = \frac{1}{Đ_i} + \frac{1}{Đ_{ii}} \\ D_{T,i} = \Gamma_i Đ_i \end{cases} \tag{4.24}$$

In conclusion, within the Maxwell-Stefan diffusion model, self- and transport diffusivities can be correlated by realizing that molecules propagating under the conditions of self-diffusion have to overcome the drag experienced by "friction" with the host lattice and the counter-diffusing molecules [15]. The reciprocal value of $Đ_{ii}$ represents the drag experienced by the guest molecules on passing each other, whereas the reciprocal value of $Đ_i$ represents the drag exerted by the confining surface on the guest molecules.

4.2.4. Water transport in carbon nanotube arrays

The apparent discrepancy between low D and high D_T of water within narrow CNTs (i.e. subnanometer diameters) may be explained by invoking the Maxwell-Stefan (M-S) diffusion model, as discussed in the previous Section [390–395]. By resorting to $Đ_i$ (M-S diffusivity, also known as corrected diffusivity) and to $Đ_{ii}$ (self-exchange coefficient) [15], it has been demonstrated that

$$\frac{1}{D} = \frac{1}{Đ_i} + \frac{1}{Đ_{ii}}. \tag{4.25}$$

In other words, self-diffusivity D within a nanoporous matrix (or, analogously, self-diffusion drag resistance $1/D$) is dictated by (a) species i-wall

and (b) species i-species i interactions, respectively [390]. Moreover, by recalling the definition of thermodynamic factor $\Gamma \equiv \frac{\partial \ln p}{\partial \ln c}$ (c is the equilibrium concentration with respect to the pressure p) [25, 394], which can be interpreted as an extra driving force for transport diffusion, transport diffusivity has been found to be correlated to the M-S one as follows:

$$D_T = \Gamma Đ_i. \tag{4.26}$$

When CNTs with subnanometer diameters are considered, single-file diffusion regime occurs, which induces a sudden increase of the drag experienced by water molecules in passing each other (i.e. $1/Đ_{ii} \to \infty$). Hence, due to Equation (4.25), $1/D \to \infty$ and D assumes near zero values, which means that water is totally nanoconfined within the CNT even if D_T may still attain quite large values [15].

Instead, when diameters larger than 1 nm are considered, Einstein-like diffusion of water is recovered. However, if CNT diameter are sized so that inner water is still predominantly under nanoconfinement conditions (i.e. wall-water interactions are significantly larger than water-water ones), $1/Đ_{ii} \ll 1/Đ_i$ [15] and Equations 4.25 and 4.26 yield $D \cong Đ_i$ thus

$$D_T \cong \Gamma D. \tag{4.27}$$

In this particular regime, self- and transport diffusivities are correlated by means of the thermodynamic factor. Equation 4.27 (also known as Darken's equation) was first suggested by Richard Barrer [396, 397], and it has been demonstrated both theoretically and experimentally to be a reliable correlation between self- and transport diffusion under the aforementioned conditions [10, 15].

For these reasons, the *a priori* prediction of self-diffusion coefficient of water within CNTs allows a more rational design of the CNA-based technologies relying on transport properties of water (e.g. mass separators, catalytic converters, selective filters, molecular sensors, nanosized chemical or biological reactors).

4.3. Carbon nanotube arrays for molecular sieves

In this Section, classical molecular dynamics simulations and the scaling law for the water transport in nanoconfined conditions presented in Chapter 2 are synergistically used for a systematic prediction of self-diffusivity of

water in CNAs, according to different pore width distributions and electrostatic fields. As an application of the theoretical and modeling evidences, a molecular sieve based on CNA is envisioned [43].

4.3.1. Water nanoconfinement in Carbon Nanotube Arrays

Water mobility is progressively reduced while approaching solid surfaces at the nanoscale, because of the confinement effect induced on water molecules by attractive nonbonded interactions at the solid-liquid interface [32]. The reduction in water mobility implies a smaller self-diffusion coefficient D, ranging from bulk values to almost null ones according to the nanoconfinement conditions, depending on the geometric, chemical and physical factors of a given configuration. Peculiar thermodynamic properties of supercooled water have a key role in interpreting the reduction of D in nanoconfined environments [17].

Following the approach in Reference [27] and widely discussed in Chapter 2, if isothermal conditions are considered, the intensity of water nanoconfinement scales with the dimensionless parameter θ (Equation 2.16). In case of CNTs immersed in homogeneous impermeable polymer or ceramic matrices, water only interacts with the inner surface of nanotubes. Hence, θ can be more precisely reformulated as:

$$\theta = \frac{\frac{\pi L}{4}\left[\phi_e^2 - (\phi_e - 2\delta)^2\right]}{\frac{\pi L}{4}\phi_e^2} = \frac{4\phi_e\delta - 4\delta^2}{\phi_e^2}, \tag{4.28}$$

being (see Figure 4.2) L the nanotube length; $\phi_e = \phi - 2h$ the solvent accessible diameter of the nanotube, where $h \approx 0.34$ nm is the minimum distance of approach between carbon atoms and water [146] and $\phi = \frac{a}{\pi}\sqrt{(n^2 + nm + m^2)}$ the nominal diameter of a nanotube, as from its chirality (n, m) with $a = 0.246$ nm. Note that, when $\delta \geq \frac{\phi_e}{2}$, water is considered as totally confined thus $\theta = 1$. By considering a CNA made out of N CNTs, the average value of the scaling parameter $\bar{\theta}$ in the composite material can be then defined as:

$$\bar{\theta} = \frac{\sum_{i=1}^{N} 4\phi_{e,i}\delta_i - 4\delta_i^2}{\sum_{i=1}^{N} \phi_{e,i}^2}. \tag{4.29}$$

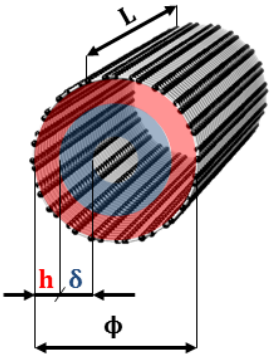

Figure 4.2.: CNT geometry. The geometric quantities of CNT, needed for evaluating the scaling parameter θ in Equation 4.28, are schematically shown. Figure adapted from Reference [43].

The quantity δ can be computed by a well defined algorithm [27] once nanoconfined geometry, Solvent Accessible Surface (SAS) of solid [173] and solid-water nonbonded interaction potentials are given (see Appendix C). SAS are generated from MD trajectories, which are produced by the following procedure: (i) CNT structures are solvated in triclinic boxes of water (SPC/E model [156]) with different volumes and periodic boundary conditions along *xyz* directions; (ii) the system made by nanotube and water is energy minimized and equilibrated; (iii) a molecular dynamics simulation of the whole setup is then performed up to 200 ps in canonical ensemble, by applying a temperature coupling on the system (time constant = 0.1 ns, T = 300 K) [398]. Two types of atomic interactions are taken into account in the simulations: i) bonded interactions, modeled as harmonic stretching and angle potentials; ii) nonbonded interactions, accounting for van der Waals and electrostatic forces, modeled as a 12-6 Lennard-Jones potential. Further details on the employed force field are reported elsewhere [27, 145–147]. Simulations are carried out with a leap-frog algorithm (1 fs time step) by means of GROMACS software [159]. Nanotubes with different size (ϕ, L) or partial charge $(q_{C,i})$ on carbon atoms are simulated, in order to assess geometric and electrostatic effects on δ.

Once θ is computed by Equation 4.28, D can be readily predicted by Equation 2.20, which can be simplified by safely assuming $\frac{D_C}{D_B} \approx 0$ [27]

and thus

$$D(\theta) \approx D_B(1-\theta), \tag{4.30}$$

namely a linear decrease of water mobility with the scaling parameter θ. In other words, since Equation 4.28 can be approximated by $\theta \approx \frac{4\phi_e\delta}{\phi_e^2}$ because usually $\phi_e \gg \delta$ thus $\frac{\delta^2}{\phi_e} \approx 0$, Equation 4.30 yields:

$$\frac{D}{D_B} \approx \left(1 - \frac{4\delta}{\phi_e}\right), \tag{4.31}$$

which is valid for $\frac{4\delta}{\phi_e} \leq 1$.

Inspection of Equation 4.31 reveals that strategies aiming at tailoring the self-diffusivity of water within CNTs can be based on the design of either the tube diameter or the confinement potential (i.e. CNT-water interactions, by introducing defects, functionalizations or external electrostatic fields).

4.3.2. Static and dynamic control of water self-diffusivity

Implications of Equation 4.31 on CNA-based technologies are analyzed by means of MD simulations, which are here used for estimating δ of CNTs in the considered setups. In particular, effects of CNT geometry or electrostatic field on D are explored, in order to suggest experimental guidelines to precisely control water self-diffusion in CNAs under static conditions [43].

First, different width distributions of CNA pores are considered. Characteristic length of nanoconfinement (δ) of CNTs are then calculated with different ϕ (i.e. from 0.8 to 14.0 nm) and L (i.e. from 5 to 50 nm) by MD simulations. Results show that nanotube geometry has no significant effect on the characteristic length of nanoconfinement, being approximately around $\delta = 0.37$ nm.

Current experimental techniques allow to produce arrays of nanotubes with size, pattern and density precisely defined, by simply adjusting production procedure or parameters [290, 362, 399]. While CNT length usually spans from tens to thousands of nanometers, CNT diameter can reach few nanometers width or even less [367, 400]. However, CNAs include pores with a Gaussian distribution of diameters ϕ, where significant standard deviations σ of the average value μ can be encountered, because

of the lack in repeatability and quality of current production techniques [367, 369, 400].

In Figure 4.3a, three Gaussian distributions of ϕ are considered (being $L = 100$ nm fixed), according to different (μ, σ) values, namely: (2.5 nm, 0.5 nm); (5.0 nm, 0.5 nm) and (2.5 nm, 1.5 nm). Note that $\phi = 0.8$ nm is the narrowest CNT experimentally observable, whereas a distribution interval $\phi \in [\mu - 2\sigma, \mu + 2\sigma]$ is taken into account. According to Equations 4.29 and 4.30 and the characteristic length of nanoconfinement δ from MD runs, overall D decreases as the average ϕ is reduced: $D\left(\bar{\theta}\right)$ is 0.99×10^{-9} m^2 s^{-1} for $\mu = 2.5$ nm (Figure 4.3b) whereas it increases to 1.78×10^{-9} m^2 s^{-1} for $\mu = 5.0$ nm (Figure 4.3c). Moreover, standard deviation has also a significant role in tailoring local and average D of water within CNAs. For example, while in CNT distribution represented in Figures 4.3b and d the mode (0.89×10^{-9} m^2 s^{-1}) and the minimum (near 0 m^2 s^{-1}) D values are the same, the maximum D shifts from 1.40×10^{-9} m^2 s^{-1} to 2.47×10^{-9} m^2 s^{-1}, respectively. Moreover, a σ increase from 0.5 to 1.5 nm leads a 40% rise in $D\left(\bar{\theta}\right)$ to 1.41×10^{-9} m^2 s^{-1}.

A more systematic analysis of the influence of μ and σ on $\bar{\theta}$ (thus on the overall D) is then performed. Results in Figure 4.4 show a synergistic contribution of μ and σ in the reduction of D. In fact, both large σ values and large μ values imply $D \approx D_B$ (regardless of other quantities); whereas if both average and standard deviation of CNT diameter distributions show lower values, an exponential reduction in D is experienced. In other words, the average D of water within CNAs can be tuned not only by controlling the average pore size (i.e. μ), but also the accuracy (i.e. σ) of the CNA production, which strongly affects the overall CNA transport properties. Note that a significant reduction (e.g. more than 25%) in overall D from bulk values is only achievable when CNT diameter distributions are characterized by $\mu < 7.0$ nm and $\sigma < 3.0$ nm. Moreover, Figure 4.4 highlights that an average bulk behavior of water within CNA-based composite materials is expected for $\phi > 10$ nm, independently from the size distribution; however, as already noticed in Figure 4.3d, highly dispersed size distributions (i.e. high σ) imply low local D, which may be of interest for size-dependent molecular sieving applications.

Second, δ and D are investigated when an electrostatic field is applied to CNA. If CNA-based composites are characterized by strong dielectric properties, the inner surface of CNTs tends to be uniformly polarized if an electrostatic field is switched on [401–403]. Therefore, MD force field

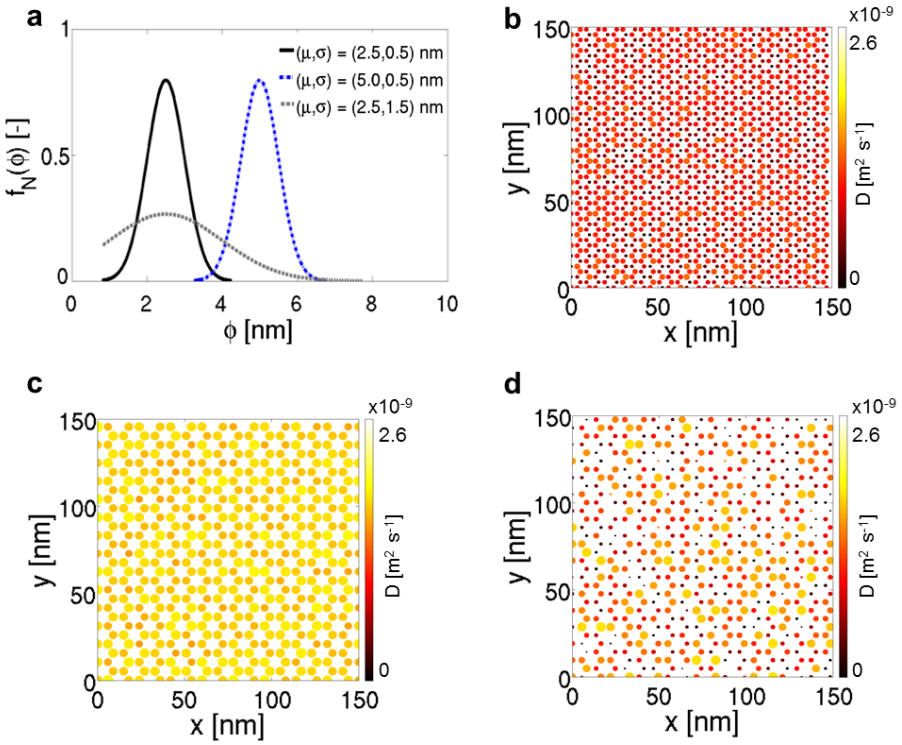

Figure 4.3.: Self-diffusivity of water in CNAs with Gaussian distribution of pore width. (a) Three Gaussian distributions of CNT diameters are considered, with different mean values μ or standard deviations σ. (b) Self-diffusion coefficient of water nanoconfined within CNTs distributed with Gaussian frequencies f_N and $\mu = 2.5$ nm, $\sigma = 0.5$ nm; (c) $\mu = 5.0$ nm, $\sigma = 0.5$ nm; (d) $\mu = 2.5$ nm, $\sigma = 1.5$ nm. Figure adapted from Reference [43].

is adequately modified for taking into account the charges introduced on carbon atoms ($q_{C,i}$) by applying an electrostatic potential to the system.

A CNT with $\phi = 1.4$ nm and $L = 12$ nm is chosen as a representative case, and δ is estimated with different $q_{C,i}$. Considering a fixed CNA section ($\mu = 2$ nm; $\sigma = 0.5$ nm), Figure 4.5 depicts how D distribution changes when $q_{C,i} = 0$ eV ($\delta = 0.37$ nm), 0.5 eV ($\delta = 0.50$ nm) or 1.0 eV ($\delta =$

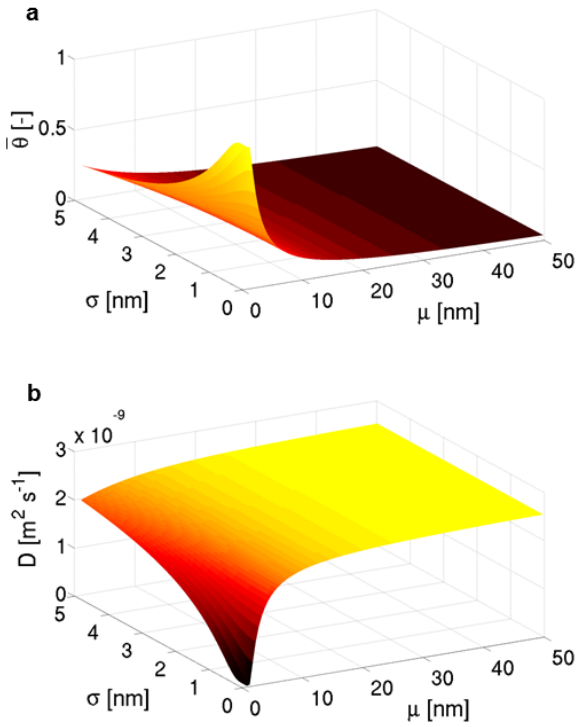

Figure 4.4.: Effect of pore diameter distribution on water nanoconfinement in CNA. (a) CNAs with Gaussian distribution of pore width are systematically analyzed ($\mu \in [0.8, 50]$; $\sigma \in [0, 5]$), and both the average scaling parameter $\bar{\theta}$ (i.e. the mean magnitude of water nanoconfinement in a CNA section) and (b) the overall self-diffusivity of entrapped water $D\left(\bar{\theta}\right)$ (Equation 4.30) are evaluated. Figure adapted from Reference [43].

0.70 nm), respectively. More specifically, $D\left(\bar{\theta}\right) = 0.70 \times 10^{-9}$ m^2 s^{-1} in a neutral CNA (Figure 4.5a), while it drops to 0.36×10^{-9} m^2 s^{-1} with $q_{C,i} =$ 0.5 eV (Figure 4.5b) and to 0.10×10^{-9} m^2 s^{-1} with $q_{C,i} = 1.0$ eV (Figure 4.5c). It is also worth mentioning that water is totally confined in 15% of CNA pores when no electrostatic field is applied (Figure 4.5d), whereas the percentage rises to 32% and 67% when $q_{C,i} = 0.5$ (Figure 4.5e) or 1.0 eV (Figure 4.5f), respectively.

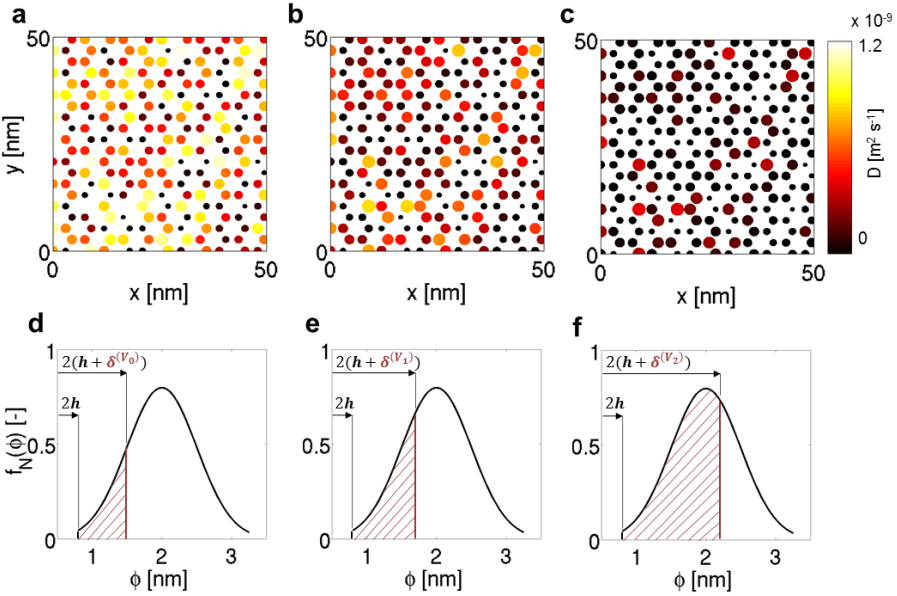

Figure 4.5.: Water nanoconfinement increase by electrostatic field application to CNA. (a) Local D of nanoconfined water are plotted as predicted by Equations 4.28 and 4.30, while considering different Coulomb charges on carbon atoms for simulating the application of an electrostatic field to CNA, namely $q_{C,i} = 0$ eV, (b) $q_{C,i} = 0.5$ eV or (c) $q_{C,i} = 1.0$ eV. (d) The considered CNA section presents pore diameters distributed with Gaussian probability ($\mu = 2.0$ nm; $\sigma = 0.5$ nm). When no electrostatic field is applied, $\delta^{(V_0)} = 0.37$ nm and 15% of CNA pores contain totally confined water (i.e. $\theta = 1$) with near zero mobility; whereas (e) with $q_{C,i} = 0.5$ eV, $\delta^{(V_1)} = 0.50$ nm and the percentage rises to 32% or, (f) with $q_{C,i} = 1.0$ eV, $\delta^{(V_2)} = 0.70$ nm and the percentage further increases to 67%. $h \approx 0.34$ nm is the minimum approaching distance between carbon atoms and water molecules. Figure adapted from Reference [43].

The voltage corresponding to an electrical charge $q_{C,i}$ can be estimated by the classical relation: $V = \frac{Q}{C}$, where $Q = \sum_i q_{C,i}$ is the overall electrostatic

charge on CNTs and C is the electrical capacitance. Experimental works show that the specific capacitance $c = \frac{C}{m}$ of pure single-walled CNTs is about 40 F g^{-1} [402]; whereas it increases to 320 F g^{-1} [404] or even more when CNTs are immersed in electrically conducting polymers, giving rise to ideal materials for supercapacitors. Hence, considering the previous upper and lower bounds for c, the voltage is found to vary within the following ranges: $V \approx 140$–1195 V for $q_{C,i} = 0.5$ eV and $V \approx 280$–2390 V for $q_{C,i} = 1$ eV, which can be easily achieved by common electrostatic devices.

Few experimental techniques are currently available for validating these predicted reductions in water self-diffusion, namely by direct (e.g. diffusion nuclear magnetic resonance – NMR [405], microimaging [15]) or indirect measurements of water dynamics under static conditions. In particular, indirect methods allow both to deduce D by measuring other physical properties of CNAs and to investigate effects of water confinement on electromagnetic, thermal or optical water properties. For example, enhancement of $r_{1,2}$ relaxivities of contrast agents for Magnetic Resonance Imaging (MRI) is inversely proportional to D [14, 210]; boiling temperature and pressure of water inside CNTs is drastically dependent on their diameter [406]; optical Kerr effect measurements are used to study modified characteristics and structures of nanoconfined water [26].

4.3.3. Carbon Nanotube Arrays as molecular sieve

Molecular dynamics simulations and theoretical arguments suggest that self-diffusion of water D within CNAs can be finely tuned, from bulk to totally confined behaviors. As from Equation 4.31, two parameters control D in CNTs, namely δ characteristic length of nanoconfinement and ϕ nanotube diameter. Different ϕ distributions in CNAs can be experimentally achieved, according to a specific pattern, surface density or width of the pores, in order to rationally design spatial D distribution of water. Nevertheless, while ϕ allows an *a priori* (i.e. passive) tuning of D (i.e. D distribution in CNAs cannot be modified once the sample is produced), the *a posteriori* (i.e. active) control of D is feasible thanks to instantaneous modifications of δ by on/off switching or tuning an external electrostatic field [43].

A broad range of CNT-based technologies may find benefits by the precise control of static transport properties of confined water molecules, in particular in biomedical or engineering fields. For example, MRI contrast

agents performances are tuned by D of nearby water molecules; whereas the delivery rate of solvated drugs encapsulated within transdermal porous materials could be also controlled by D of surrounding water, both in constant release applications (e.g. long-term administration of therapeutics) and in dynamic ones (e.g. drug release in response to sudden pathological conditions). Moreover, the value of D in water is a key parameter in molecular sensors, sieves and biological/chemical reaction chambers.

As an example, in Figure 4.6 we report the functional scheme of a possible molecular sieve based on *a posteriori* control (by electrostatic field) of D within a CNA-based composite. CNA should be adequately engineered with a ϕ size distribution so that only nanoparticles/molecules with approximately $\phi_p < \phi_e - 2\delta$ diameter could pass through its nanopores (red and green spheres in Figure 4.6a). Note that chemical functionalization of both nanoparticles and CNTs may also influence the permeability of molecular sieve. Once an electrostatic field is applied to the CNA thus δ increases to $\delta^{(V)}$, sieving properties could suddenly change, due to reduced mobility of water within CNAs. For example, bigger nanoparticles/molecules could be trapped in the porous matrix (red spheres in Figure 4.6b), which could become partially or totally impermeable to nanoparticles/molecules with approximately $\phi_p > \phi_e - 2\delta^{(V)}$ diameters. In fact, if CNA membranes are designed with well-defined pore sizes such that Barrer's approximation holds and self- and transport diffusivities can be correlated by Darken's equation (Equation 4.27), the increase in low-mobility water volume within CNTs may in turn affect the dynamic transport properties of CNA [43].

4.4. Conclusions

In this Chapter, self-diffusion coefficient D of water within carbon nanotube arrays is numerically studied, while theoretical considerations are formulated for better understanding the relation between self- and transport diffusivities. D is found to scale with CNT diameter ϕ and characteristic length of nanoconfinement δ, which is related to the solid-liquid nonbonded interaction potential at the interface. A strategy for an *a priori* (i.e. passive) modulation of D in CNA-based applications is suggested, by controlling size distribution of the pore widths. Moreover, δ of CNTs can be increased by introducing electrostatic field thus allowing also an *a posteriori* (i.e. active) control of D in CNAs. If the Barrer approximation is considered, also transport diffusivity D_T should modify its magnitude by following the D modulation.

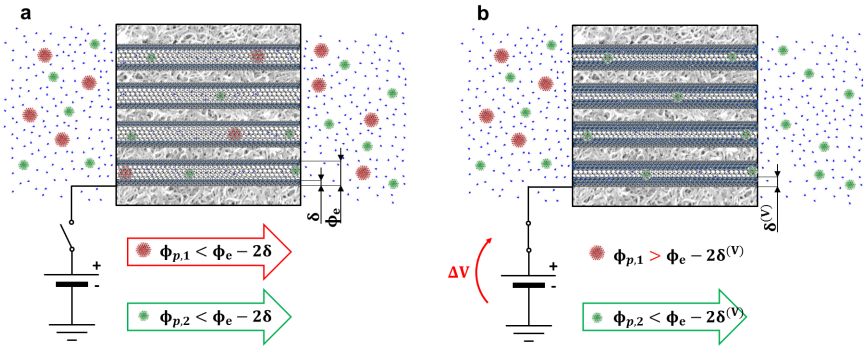

Figure 4.6.: Schematics of a tunable/switchable molecular sieve based on CNA. (a) CNA-based composites may be used for sieving purposes, because their tunable pore width distribution induces different mass transport properties within pores. Thanks to Equations 4.28 and 4.30, CNA-based sieves may be designed for being selectively permeable to different nanoparticles or molecules, according to their size and chemical functionalization. (b) Sieving properties may also be influenced by the application of electrostatic field on CNA, which enhances δ of CNTs thus slowing down water dynamics and overall mass transport properties of the sieve. Hence, permeation features of CNAs may be precisely tuned and dynamically switched. Figure adapted from Reference [43].

A large variety of fields may benefit from a precise control of transport properties of water entrapped within CNA-based technologies, such as nanomedicine and environmental or energy engineering.